bioRxiv preprint doi: https://doi.org/10.1101/137299; this version posted May 12, 2017. The copyright holder for this preprint (which was not certified by peer review) is the author/funder, who has granted bioRxiv a license to display the preprint in perpetuity. It is made available under aCC-BY 4.0 International license.

Ratiometric distribution of OCT4 during stem cell division controls the balance between self-renewal and differentiation

Samuel C. Wolff[1]*, Raluca Dumitru[1]*, Cierra D. Dungee[1], Katarzyna M. Kedziora[1], Rachel A. Haggerty[2], JrGang Cheng[3], Adriana S. Beltran[1], and Jeremy E. Purvis[1,2,4,†]

[1]Department of Genetics
[2]Curriculum for Bioinformatics and Computational Biology
[3]UNC Neuroscience Center
[4]Lineberger Comprehensive Cancer Center

University of North Carolina, Chapel Hill
120 Mason Farm Road
Chapel Hill, NC 27599-7264

*These authors contributed equally

[†]Corresponding Author:
Jeremy Purvis
Genetic Medicine Building 5061, CB#7264
120 Mason Farm Road
Chapel Hill, NC 27599-7264
jeremy_purvis@med.unc.edu

bioRxiv preprint doi: https://doi.org/10.1101/137299; this version posted May 12, 2017. The copyright holder for this preprint (which was not certified by peer review) is the author/funder, who has granted bioRxiv a license to display the preprint in perpetuity. It is made available under aCC-BY 4.0 International license.

A fundamental challenge in cell biology is to understand how an individual cell commits to a particular fate[1-3]. A classic example is the fate decision between self-renewal and differentiation, which plays an essential role in the biology of human embryonic stem cells (hESCs)[4]. Despite significant advances in our understanding of development of the human embryo[5,6], it is still unclear how, and when, an individual stem cell makes the decision to differentiate. Here, we used time-lapse fluorescence microscopy to capture differentiation of hESCs to trophoblast—the first cell fate decision during mammalian development. By tracing the histories of both self-renewing and differentiating cells, we found that each population displayed distinct levels of the pluripotency factor OCT4 long before they were exposed to a differentiation stimulus. The levels of OCT4 were lineage dependent; however, each mother cell distributed unequal levels of OCT4 to its daughter cells randomly during cell division. The resulting ratio of OCT4 between daughter cells—established immediately after division—determined downstream fates: cells receiving a greater ratio of maternal OCT4 showed sustained increases in OCT4 and a reduced capacity to differentiate. We propose a simple formula, $p_{daughter} = (p_{mother})^r$, that successfully predicts the probability that a daughter cell will differentiate based on its mother cell's differentiation probability and its inherited ratio of OCT4. Our study reveals that the balance between self-renewal and differentiation is altered by the ratiometric distribution of OCT4 during cell division. These findings imply that a stem cell's fate is already largely determined by the time the cell is born.

In the early human embryo, hESCs give rise to either pluripotent cells of the inner cell mass that will form the embryo proper, or extraembryonic trophoblast cells that will become placental tissue[5,7]. Differentiation of hESCs to trophoblasts leads to reduced expression of the core pluripotency factor OCT4 and accumulation of the caudal type homeobox 2 (CDX2) transcription factor (**Fig. 1a**)[5,8]. This cellular fate decision can be recapitulated *in vitro* by treating hESCs with

bioRxiv preprint doi: https://doi.org/10.1101/137299; this version posted May 12, 2017. The copyright holder for this preprint (which was not certified by peer review) is the author/funder, who has granted bioRxiv a license to display the preprint in perpetuity. It is made available under aCC-BY 4.0 International license.

bone morphogenetic protein 4 (BMP4)[9]. After 24 h of BMP4 treatment, quantitative immunofluorescence (IF) reveals two emerging populations of cells: a pluripotent population with low CDX2 expression that retains the ability to differentiate into other cell types (**Extended Data Fig. 1**); and a differentiating population of cells with reduced OCT4 expression, increased CDX2 expression, and enlarged morphology (**Figs. 1b-c**). BMP4-treated hESC colonies adopted a radially symmetric pattern of differentiation that resembles the human gastrula[10] (**Extended Data Fig. 2**). This spatial configuration—with pluripotent cells located at the interior of the colony and differentiated cells near the periphery—was recently shown to arise from a gradient of receptor polarization and diffusible factors[6]. However, the self-organization of a seemingly uniform starting population still raises the fundamental question: how does a single stem cell choose between self-renewal and differentiation?

To address this question, we developed a fluorescent reporter system to monitor expression of human OCT4, a canonical marker of the pluripotent state[11], in live hESCs. We used CRISPR-mediated genome editing to fuse a monomeric red fluorescent protein (mCherry) to the endogenous OCT4 protein in WA09 (H9) hESCs and isolated a clonal population of single-allele knock-in reporter cells (**Fig. 1d** and **Extended Data**). The OCT4-mCherry fusion protein showed accurate co-localization with the endogenous OCT4 protein; similar degradation kinetics; and the same chromatin binding pattern near the promoters of OCT4 target genes (**Extended Data Fig. 3**). Moreover, cells bearing the OCT4-mCherry reporter were competent to differentiate into multiple differentiated cell types (**Extended Data Fig. 4**), and time-lapse imaging did not alter their proliferation characteristics (**Extended Data Fig. 5**). For each cell, we calculated a single OCT4 expression level by averaging OCT4-mCherry intensity over its cell cycle duration (**Fig. 1e-f**). In addition, we examined the time-series profile of OCT4 dynamics for individual cells and found that the majority of hESCs (68%) displayed sporadic bursts of OCT4 expression that lasted ~1.5 h, with some cells showing as many as 7 bursts (**Fig. 1g**). Finally, we calculated individual cell cycle durations, which ranged from 10-24 h with a mean duration of

bioRxiv preprint doi: https://doi.org/10.1101/137299; this version posted May 12, 2017. The copyright holder for this preprint (which was not certified by peer review) is the author/funder, who has granted bioRxiv a license to display the preprint in perpetuity. It is made available under aCC-BY 4.0 International license.

14.6 h (**Fig. 1h**), consistent with the reported population doubling time of ~16 h[12]. Thus, our reporter system enabled the reliable analysis of single-cell OCT4 dynamics in hESCs and revealed considerable heterogeneity in untreated stem cells.

With this system in place, we set out to capture the fate decisions of hESCs in real time. First, we performed time-lapse fluorescence imaging of H9 OCT4-mCherry hESCs for 42 h under basal conditions (**Fig. 2a**). We then treated these cells with 100 ng/mL BMP4 to induce differentiation while continuing to monitor their responses. Within 12 h of treatment, each cell began to follow one of two distinct fate paths: sustained accumulation of OCT4; or a precipitous decrease in OCT4. After 24 h, cells were fixed and stained for expression of CDX2 to determine their final differentiation status (**Fig. 2b**). We imposed a strict cutoff to classify each cell as either pluripotent or differentiated based on its OCT4 and CDX2 expression levels. By fitting the data in **Fig. 2b** to a 2-component Gaussian distribution (**Extended Data Fig. 6**), we selected only those cells that belonged exclusively to either the pluripotent distribution ($p_{diff} < 0.01$) or the differentiated distribution ($p_{diff} > 0.99$), where p_{diff} represents the probability that a given cell has differentiated. We then traced both populations back through time—spanning multiple cell division events—and labeled each earlier cell according to its “pro-fate”—the fate to which it (or its progeny) would ultimately give rise. The majority of cells were either pro-pluripotent (71%, red traces in **Fig. 2a**), giving rise to only self-renewing cells; or pro-differentiated (24%, green traces in **Fig. 2a**), giving rise to only differentiated cells. Approximately 5% of cells were “pro-mixed” and gave rise to both fates (yellow traces in **Fig. 2a)**. Overall, 89% of sister cells chose the same fate, suggesting a large degree of heritability in cell fate and the absence of classically described “asymmetric” cell divisions[13]. Thus, time-lapse imaging allowed us to group hESCs by their eventual fate categories before they had received a differentiation signal or had made a clear fate decision. Although the majority of progenitor cells gave rise exclusively to a single fate, a small but significant group of cells gave rise to two different fates.

bioRxiv preprint doi: https://doi.org/10.1101/137299; this version posted May 12, 2017. The copyright holder for this preprint (which was not certified by peer review) is the author/funder, who has granted bioRxiv a license to display the preprint in perpetuity. It is made available under aCC-BY 4.0 International license.

We next asked whether there were preexisting differences between pro-pluripotent, pro-mixed, and pro-differentiated cell populations that might influence their fate decisions. Indeed, pro-pluripotent cells showed significantly higher OCT4 expression levels than either pro-differentiated or pro-mixed populations (**Fig. 2c**). This result echoes the observation that repression of Oct4 in mouse ESCs induces loss of pluripotency and differentiation to trophectoderm[14]. Pro-pluripotent cells also showed greater burst frequency (number of OCT4 bursts per hour) than pro-mixed cells (**Fig. 2d**) and had shorter cell cycle durations than both pro-mixed and pro-differentiated populations (**Fig. 2e**). The latter finding is consistent with reports that hESC self-renewal is linked with a shortened G1 cell cycle phase[15]. Furthermore, we observed that both burst frequency and cell cycle duration were strongly correlated with mean OCT4 levels (**Fig. 2f-g**). Taken together, these results show that undifferentiated hESCs display heterogeneous OCT4 levels, burst dynamics, and cell cycle durations. These single-cell features, which were evident as early as 2 days before the differentiation stimulus was presented, were associated with alternate cell fate decisions. Although the preexisting differences between pro-fate populations were statistically significant, these populations of cells still showed considerable heterogeneity and overlapping measurements, suggesting that there are additional factors or events that influence final cell fate.

Because OCT4 levels were the strongest predictors of cell fate (**Fig. 2c**), we next asked how heterogeneity in OCT4 levels arises in a population of hESCs. To identify the source of cell-to-cell heterogeneity, we monitored OCT4 expression continuously in proliferating, undifferentiated hESCs for 72 h and generated lineage trees of single-cell relationships (**Fig. 3a**). Visual inspection of the lineages revealed that OCT4 levels were most similar among closely related cells (i.e., cells emerging from a common cell division event), providing further support that OCT4 levels are heritable from mother to daughter cell. To quantify this heritability pattern, we calculated the differences in OCT4 levels between pairs of cells as a function of their shared history. Sister cells showed the most similarity in OCT4 levels, followed by “cousin”

bioRxiv preprint doi: https://doi.org/10.1101/137299; this version posted May 12, 2017. The copyright holder for this preprint (which was not certified by peer review) is the author/funder, who has granted bioRxiv a license to display the preprint in perpetuity. It is made available under aCC-BY 4.0 International license.

and "second cousin" cells (**Fig. 3b**). Both sister and cousin cells, but not second cousins, were more similar than randomly paired cells, indicating that similarity in OCT4 levels can persist for at least two cell cycle generations[16]. Suspecting that each cell division event introduced variability in OCT4 levels, we detected a strong correlation between the number of cell divisions and the difference in OCT4 levels between all pairs of cells (**Extended Data Fig. 7**). Thus, OCT4 levels are heritable from mother to daughter cell, but each division event introduces incremental variability in OCT4 expression levels.

Close examination of cell division events at high temporal resolution revealed the precise time during which variability in OCT4 levels arises during cell division. As cells entered mitosis, OCT4 became strongly associated with the condensed chromosomes (**Fig. 3c**, *left panel*). This compacted state persisted throughout anaphase until the two daughter chromatids could be visibly distinguished. We used this first time point—before cytokinesis was complete—to quantify the levels of OCT4 in both newly born daughter cells (**Fig. 3c**, *center panel*). Comparison of OCT4-mCherry intensity between daughter cells revealed that the distribution of OCT4 was not perfectly symmetric but instead adopted a bell-shaped distribution that was centered around a mean ratio of 1 ($r = 1/1$) (**Fig. 3d**). Approximately 38% of divisions produced daughter cells with $r = 5/6$ or a more extreme ratio; 12% of divisions resulted in $r = 3/4$ or a more extreme ratio; and 3% of division events resulted in $r = 1/2$ or a more extreme ratio. These differences in OCT4 ratios were not due to measurement error because the distribution of r between sisters remained consistent for several hours after cytokinesis both before and after BMP4 treatment (see below). In addition, we determined the half-life of OCT4 to be ~8 h (**Extended Data Fig. 3**), making it unlikely that asymmetric ratios were due to stochastic differences in protein degradation during the first 5 minutes of daughter cell lifetime. Moreover, OCT4 ratios were not correlated with nuclear area or radial position within the colony (**Extended Data Fig. 8**). Thus, significant differences in OCT4 protein levels between sister-cell pairs were established at the moment of cell division.

bioRxiv preprint doi: https://doi.org/10.1101/137299; this version posted May 12, 2017. The copyright holder for this preprint (which was not certified by peer review) is the author/funder, who has granted bioRxiv a license to display the preprint in perpetuity. It is made available under aCC-BY 4.0 International license.

We next tested whether the ratio of OCT4 inherited by a particular daughter cell influenced its downstream behavior. By comparing OCT4-mCherry intensities between sister chromatids at the moment of cell division, we found that the inherited ratio of OCT4 established within the first 5 minutes of daughter cell separation was predictive of the final OCT4 level in each cell (**Fig. 3e**). Daughter cells receiving the larger proportion of OCT4 ($r > 1$) showed increased levels of OCT4 relative to the mother cell, whereas daughters receiving the smaller proportion of OCT4 ($r < 1$) showed permanent decreases in OCT4. This trend was also observed after differentiation (**Fig. 3e**, *right panel*) and became stronger as more time elapsed after cell division (**Extended Data Fig. 9**). Furthermore, the ratio of OCT4 immediately after division predicted the difference in final OCT4 expression between sister cell pairs (**Extended Data Fig. 10**). Thus, the ratio of OCT4 established immediately after cell division—before the nuclear envelope is formed—determined the amount of OCT4 that was maintained throughout the lifetime of a cell.

To summarize thus far, differences in OCT4 expression levels arise through asymmetric distribution of OCT4 to daughter cells (**Fig. 3c-e**). Precise levels of OCT4 are transmitted from mother to daughter cells as reflected by both the similarity among cells that share a common lineage (**Fig. 3a-b**) as well as the observation that most progenitor cells (89%) give rise to a group of cells with the same fate (**Fig. 2a**). Moreover, OCT4 levels are strongly predictive of cell fate decisions (**Fig. 2c**). Taken together, these results suggest that a cell's probability of differentiation has both a heritable component—transmitted through the mother cell—and a random component that depends on the inherited ratio of OCT4 at the moment of cell division. This behavior can be expressed in a simple formula (**Fig. 4a**) in which the probability that a daughter cell will differentiate, $p_{daughter}$, is equal to the probability that its mother cell will give rise to differentiated cells, p_{mother}, raised to the power of r, the inherited ratio of OCT4:

$$p_{daughter} = (p_{mother})^r \qquad \textbf{Equation 1}$$

bioRxiv preprint doi: https://doi.org/10.1101/137299; this version posted May 12, 2017. The copyright holder for this preprint (which was not certified by peer review) is the author/funder, who has granted bioRxiv a license to display the preprint in perpetuity. It is made available under aCC-BY 4.0 International license.

Here, $p_{daughter}$ can represent either the probability that a daughter cell has differentiated (as shown in **Fig. 2b**) or the probability that the daughter cell will give rise to differentiated daughter cells (i.e., pro-differentiated, green circles in **Fig. 2c**). As such, **Equation 1** is a recursive formula that can be used to assign a probability to every cell in a lineage tree. By fitting **Equation 1** to our measured values of p_{diff} and r, we assigned a differentiation probability to each cell in a proliferating population including those cells that were observed before the differentiation stimulus was given (**Fig. 4b**). As expected, pro-pluripotent cells had the lowest differentiation probabilities ($p < 0.5$), pro-differentiated cells the highest differentiation probabilities ($p > 0.5$), and pro-mixed cells had intermediate differentiation probabilities ($0.2 < p < 0.8$).

Because all probabilities lie between 0 and 1 ($p_{daughter}, p_{mother} \in [0,1]$) and because the OCT4 ratio is always a positive rational number ($r \in \mathbb{Q}^+$), **Equation 1** has the following desirable properties: (*i*) As less OCT4 is inherited by a daughter cell ($r \to 0$), it becomes more likely to differentiate ($p_{daughter} \to 1$). (*ii*) As more OCT4 is inherited by the daughter cell ($r \to \infty$), it becomes less likely to differentiate ($p_{daughter} \to 0$). (*iii*) If OCT4 is split evenly between daughter cells ($r = 1$), each daughter cell has the same differentiation potential as the mother cell ($p_{daughter} = p_{mother}$). Theoretical predictions of **Equation 1** are illustrated in **Fig. 4c**. Each line shows how the differentiation probability of a daughter cell, $p_{daughter}$, changes as a function of the mother cell's differentiation probability, p_{mother}, and the inherited ratio of OCT4, r. For example, when the mother cell is likely to differentiate ($p \approx 0.9$), a $1/2$ ratio of OCT4 inherited by a pair of daughter cells should alter their differentiation probabilities by ~10%. Given the experimentally measured distribution of OCT4 ratios (blue shading in **Fig. 4c**), in which only 3% of cells inherit ratios in this extreme range (**Fig. 3d**), **Equation 1** provides an explanation for why only 5% of cells gave rise to both pluripotent and self-renewing cell fates (pro-mixed group

bioRxiv preprint doi: https://doi.org/10.1101/137299; this version posted May 12, 2017. The copyright holder for this preprint (which was not certified by peer review) is the author/funder, who has granted bioRxiv a license to display the preprint in perpetuity. It is made available under aCC-BY 4.0 International license.

in **Fig. 2a**). In other words, the fairly narrow distribution of OCT4 ratios observed experimentally accounts for why most daughter cells choose the same fate.

However, **Equation 1** also makes an unexpected prediction. **Fig. 4c** indicates that cells with intermediate differentiation probabilities, such as the pro-mixed group, should be especially sensitive to the inherited ratio of OCT4 (note that the slopes of the curves in **Fig. 4c** are steepest at $r = 1$ for $p = 0.25$ and $p = 0.5$) whereas cells that are already likely to differentiate (p near 1) should be relatively insensitive to r. We tested this prediction by comparing the change in final OCT4 levels versus inherited ratios in the pro-pluripotent, pro-mixed, and pro-differentiated populations. In fact, the pro-mixed population showed the most sensitivity to OCT4 ratio while the pro-differentiated population showed the least sensitivity (**Fig. 4d**). Mechanistically, this increase in sensitivity to OCT4 at intermediate levels is consistent with the finding that the OCT4 and CDX2 transcription factors are reciprocally inhibitory[8]. Such a "double-negative feedback loop" would lead to a bistable system[17] in which a small change in OCT4 levels drives cells strongly toward either pluripotency or differentiation (**Fig. 4e**).

In conclusion, we developed an endogenous fluorescent reporter for the canonical pluripotency factor OCT4 to capture differentiation of human embryonic stem cells in real time. We found that the decision to differentiate to trophoblast is largely determined before the differentiation stimulus is presented to cells and can be predicted by a cell's preexisting OCT4 levels, bursting frequency, and cell cycle duration. These results in human cells harmonize with studies of mouse ESCs in which differences in OCT4 expression[14,18-20] and degradation kinetics[21,22] are associated with different developmental fate decisions. However, we identify a precise window of time during which these differences arise by showing that the strongest predictor of trophoblast fate—OCT4 levels—is established during cell division through ratiometric distribution of OCT4 to daughter cells. Thus, a cell's probability to differentiate is a mixture of both heritable and random components. These observations challenge a prevailing view of cell fate decisions by suggesting that the fate of a cell is already largely determined by

bioRxiv preprint doi: https://doi.org/10.1101/137299; this version posted May 12, 2017. The copyright holder for this preprint (which was not certified by peer review) is the author/funder, who has granted bioRxiv a license to display the preprint in perpetuity. It is made available under aCC-BY 4.0 International license.

the time it emerges from its mother cell. As such, the concept of pluripotency—currently defined as the capacity of a given cell to undergo differentiation—may be more properly comprehended as a heritable trait that applies to an entire lineage of proliferating stem cells.

ACKNOWLEDGEMENTS

We thank Paul Lerou, Galit Lahav, Allon Klein, Jean Cook, Paul Maddox, Bill Marzluff, Scott Bultmann, Peijie Sun, and members of the Purvis Lab for helpful discussions and technical suggestions. This work was supported by NIH grant DP2-HD091800-01, the W.M. Keck Foundation, and the Loken Stem Cell Fund.

AUTHOR CONTRIBUTIONS

S.C.W., R.D., and J.C. constructed the OCT4-mCherry reporter cell line. S.C.W. and R.D. performed validation studies. S.C.W. and C.D. performed live-cell imaging. C.D., R.A.H., and K. K. conducted image analysis and cell tracking. C.D., R.A.H., and J.E.P. performed computational analysis. S.C.W. and A.S.B. carried out lineage differentiation experiments. J.E.P wrote the manuscript with contributions from all authors.

FIGURE LEGENDS

Figure 1 | Single-cell dynamics of OCT4 in human embryonic stem cells. a, Individual hESCs have the potential to generate another stem cell through self-renewal or to differentiate into a more lineage-specific cell type. The first fate decision during human development leads to separation of a pluripotent inner cell mass (OCT4+/CDX2-) and a population of differentiated trophoblast cells (OCT4-/CDX2+). **b**, Before differentiation, hESCs show uniform expression of OCT4. Treatment with BMP4 produces a mixture of OCT4+/CDX2- pluripotent hESCs and OCT4-/CDX2+ trophoblast cells. **c**, Quantification of OCT4 and CDX2 expression by

bioRxiv preprint doi: https://doi.org/10.1101/137299; this version posted May 12, 2017. The copyright holder for this preprint (which was not certified by peer review) is the author/funder, who has granted bioRxiv a license to display the preprint in perpetuity. It is made available under aCC-BY 4.0 International license.

immunofluorescence after 24 h of BMP4 treatment reveals two populations of hESCs. **d**, A fluorescent mCherry coding sequence was introduced into endogenous OCT4 locus of H9 hESCs using CRISPR-mediated homologous recombination. **e**, Filmstrip of OCT4 dynamics in an undifferentiated hESC throughout its cell cycle duration. Yellow outlines indicate the region used to quantify mean nuclear fluorescence intensity. **f**, Distribution of OCT4 levels in individual hESCs. A single OCT4 level was quantified for each cell by averaging the mCherry intensity over the lifetime of the cell. **g**, Single-cell traces of OCT4 signaling. The length of each cell's trace indicates its cell cycle duration. **h**, Distribution of cell cycle durations for 120 hESCs.

Figure 2 | Preexisting differences in OCT4 dynamics predict eventual fate decisions. a, Single-cell traces of hESCs before and after treatment with 100 ng/mL BMP4. Cells were imaged for 42 h prior to BMP4 treatment. Mean nuclear OCT4 levels were quantified every 5 minutes and individual cells were tracked from the cell division event that created the cell until its own division. **b**, 24 h after BMP4 treatment, cells were fixed, stained for expression of CDX2, and returned to the microscope for registration with the final time-lapse image. Mean nuclear OCT4-mCherry and CDX2 were quantified for each cell, and the resulting distribution was fit to a 2-component mixed Gaussian distribution representing pluripotent (OCT4+/CDX2-) and differentiated (OCT4-/CDX2+) cells (**Extended Data Fig. 6**). hESCs that could be assigned to either distribution with >99% confidence (red and green dots, $p_{diff} < 0.01$ or $p_{diff} > 0.99$) were considered for pro-fate analysis. Cells that did not reach this threshold (gray dots) were not used to determine pro-fate. **c**, Distributions of OCT4 levels in pro-pluripotent, pro-mixed, and pro-differentiated cell populations. **d**, Distributions of OCT4 burst frequencies in pro-pluripotent, pro-mixed, and pro-differentiated cell populations. **e**, Distributions of cell cycle durations in pro-pluripotent, pro-mixed, and pro-differentiated cell populations. To gain an unbiased look at preexisting determinants of cell fate in panels **d**-**e**, only cells who completed their entire cell cycle duration before BMP4 addition (t = 0) were included in the analysis. **f**, Correlation between

bioRxiv preprint doi: https://doi.org/10.1101/137299; this version posted May 12, 2017. The copyright holder for this preprint (which was not certified by peer review) is the author/funder, who has granted bioRxiv a license to display the preprint in perpetuity. It is made available under aCC-BY 4.0 International license.

OCT4 level and burst frequency across the entire population of pro-fate cells. **g**, Correlation between OCT4 level and cell cycle duration across the entire population of pro-fate cells. * $p < 0.05$, ** $p < 0.005$, *** $p < 0.0005$, two-sample Kolmogorov-Smirnov test; ns, not significant. *r*, Pearson correlation; *p*, *p*-value.

Figure 3 | Differences in OCT4 expression levels arise through asymmetric distribution of OCT4 to daughter cells. a, Lineage of OCT4 expression dynamics. Mean nuclear OCT4 levels were quantified in individual hESCs continuously for 72 h under undifferentiated conditions. Vertical bars represent individual cells. Thin horizontal bars denote cell division events. Color scale indicates low (*black*), intermediate (*red*), and high (*white*) OCT4 expression levels. **b,** Differences in OCT4 levels between sister cells, cousin cells, second cousin cells, and randomly paired cells. **c,** Filmstrip showing distribution of OCT4 to daughter cells during cell division. **d,** Distribution of OCT4 ratios between sister cells before and after BMP4 treatment. Ratios for both sister cells (r and $1/r$) are plotted to emphasize symmetry. Differently colored curves represent the distribution of ratios at different time points after division. For time points after 5 minutes, the ratio was determined by first calculating a mean OCT4 level for each sister cell among all previous time points and then calculating the resulting ratio between sisters. **e,** Correlation between OCT4 ratio established within 5 minutes of cell division and the final OCT4 level. To avoid trivial correlations, OCT4 measurements used to determine the ratio (x-axis) were excluded from the final OCT4 level calculation (y-axis). F * $p < 0.05$, ** $p < 0.005$, *** $p < 0.0005$, two-sample Kolmogorov-Smirnov test; ns, not significant. *r*, Pearson correlation; *p*, *p*-value; *m*, slope of best fit line. Results are representative of at least 3 independent experiments.

Figure 4 | Ratiometric distribution of OCT4 during cell division alters the balance between self-renewal and differentiation. a, Formula that describes how the differentiation probability of a daughter cell $p_{daughter}$ depends on the differentiation probability of the mother

bioRxiv preprint doi: https://doi.org/10.1101/137299; this version posted May 12, 2017. The copyright holder for this preprint (which was not certified by peer review) is the author/funder, who has granted bioRxiv a license to display the preprint in perpetuity. It is made available under aCC-BY 4.0 International license.

cell p_{mother} and the inherited ratio of OCT4 r. **b,** **Equation 1** was used to recursively assign a differentiation probability to each cell based on the final measured differentiation probability p_{diff} (see **Fig. 2b**) and the inherited ratio of OCT4 for each cell. Cells are grouped according to their experimentally determined pro-fate. **c,** Theoretical predictions of **Equation 1** for multiple values of maternal differentiation probability p_{mother}. The line is steepest at $p_{mother} = 1/e \approx 0.368$. **d,** Sensitivity of pro-fate groups to inherited OCT4 ratio. The change in final OCT4 levels is plotted against the ratio of OCT4 inherited in pro-pluripotent, pro-mixed, and pro-differentiated populations. **e,** Model for stem cell fate decisions altered by asymmetric distribution of OCT4 during cell division. *r*, Pearson correlation; *p*, *p*-value; *m*, slope of best fit line.

REFERENCES

1 Suel, G. M., Garcia-Ojalvo, J., Liberman, L. M. & Elowitz, M. B. An excitable gene regulatory circuit induces transient cellular differentiation. *Nature* **440**, 545-550 (2006).

2 Purvis, J. E. *et al.* p53 dynamics control cell fate. *Science* **336**, 1440-1444 (2012).

3 Spencer, S. L. *et al.* The proliferation-quiescence decision is controlled by a bifurcation in CDK2 activity at mitotic exit. *Cell* **155**, 369-383 (2013).

4 He, S., Nakada, D. & Morrison, S. J. Mechanisms of stem cell self-renewal. *Annu Rev Cell Dev Biol* **25**, 377-406 (2009).

5 Deglincerti, A. *et al.* Self-organization of the in vitro attached human embryo. *Nature* **533**, 251-254 (2016).

6 Etoc, F. *et al.* A Balance between Secreted Inhibitors and Edge Sensing Controls Gastruloid Self-Organization. *Developmental cell* **39**, 302-315 (2016).

7 Shahbazi, M. N. *et al.* Self-organization of the human embryo in the absence of maternal tissues. *Nat Cell Biol* **18**, 700-708 (2016).

8 Niwa, H. *et al.* Interaction between Oct3/4 and Cdx2 determines trophectoderm differentiation. *Cell* **123**, 917-929 (2005).

9 Xu, R. H. *et al.* BMP4 initiates human embryonic stem cell differentiation to trophoblast. *Nature biotechnology* **20**, 1261-1264 (2002).

bioRxiv preprint doi: https://doi.org/10.1101/137299; this version posted May 12, 2017. The copyright holder for this preprint (which was not certified by peer review) is the author/funder, who has granted bioRxiv a license to display the preprint in perpetuity. It is made available under aCC-BY 4.0 International license.

10 Warmflash, A., Sorre, B., Etoc, F., Siggia, E. D. & Brivanlou, A. H. A method to recapitulate early embryonic spatial patterning in human embryonic stem cells. *Nat Methods* **11**, 847-854 (2014).

11 Nichols, J. *et al.* Formation of pluripotent stem cells in the mammalian embryo depends on the POU transcription factor Oct4. *Cell* **95**, 379-391 (1998).

12 Ghule, P. N. *et al.* Reprogramming the pluripotent cell cycle: restoration of an abbreviated G1 phase in human induced pluripotent stem (iPS) cells. *J Cell Physiol* **226**, 1149-1156 (2011).

13 Morrison, S. J. & Kimble, J. Asymmetric and symmetric stem-cell divisions in development and cancer. *Nature* **441**, 1068-1074 (2006).

14 Niwa, H., Miyazaki, J. & Smith, A. G. Quantitative expression of Oct-3/4 defines differentiation, dedifferentiation or self-renewal of ES cells. *Nat Genet* **24**, 372-376 (2000).

15 Becker, K. A. *et al.* Self-renewal of human embryonic stem cells is supported by a shortened G1 cell cycle phase. *J Cell Physiol* **209**, 883-893 (2006).

16 Spencer, S. L., Gaudet, S., Albeck, J. G., Burke, J. M. & Sorger, P. K. Non-genetic origins of cell-to-cell variability in TRAIL-induced apoptosis. *Nature* **459**, 428-432 (2009).

17 Ferrell, J. E., Jr. & Ha, S. H. Ultrasensitivity part III: cascades, bistable switches, and oscillators. *Trends in biochemical sciences* **39**, 612-618 (2014).

18 Zeineddine, D. *et al.* Oct-3/4 dose dependently regulates specification of embryonic stem cells toward a cardiac lineage and early heart development. *Developmental cell* **11**, 535-546 (2006).

19 Radzisheuskaya, A. *et al.* A defined Oct4 level governs cell state transitions of pluripotency entry and differentiation into all embryonic lineages. *Nat Cell Biol* **15**, 579-590 (2013).

20 Goolam, M. *et al.* Heterogeneity in Oct4 and Sox2 Targets Biases Cell Fate in 4-Cell Mouse Embryos. *Cell* **165**, 61-74 (2016).

21 Filipczyk, A. *et al.* Network plasticity of pluripotency transcription factors in embryonic stem cells. *Nat Cell Biol* **17**, 1235-1246 (2015).

22 Plachta, N., Bollenbach, T., Pease, S., Fraser, S. E. & Pantazis, P. Oct4 kinetics predict cell lineage patterning in the early mammalian embryo. *Nat Cell Biol* **13**, 117-123 (2011).

bioRxiv preprint doi: https://doi.org/10.1101/137299; this version posted May 12, 2017. The copyright holder for this preprint (which was not certified by peer review) is the author/funder, who has granted bioRxiv a license to display the preprint in perpetuity. It is made available under aCC-BY 4.0 International license.

METHODS

Culture and treatment of hESCs. WA09 (H9) hES cell line was purchased from WiCell (Wisconsin) and maintained in mTeSR1 (05850, StemCell Technologies) on growth factor reduced Matrigel (354230, BD). Cells were passaged every three days using 0.5% EDTA in PBS.

Genome editing. H9 cells were cultured on 10 cm dishes and when 80% confluent, were dissociated using 0.5mM EDTA. 10×10^6 cells were resuspended in 800ul ice-cold PBS-/- containing 25ug of the OCT4-mCherry donor vector and 25ug of the guideRNA/Cas9 vector. Cells were electroporated in 100ul tips (Neon, ThermoFisher Scientific) using program 19 of the optimization protocol (1050V, 30ms and 2 pulses) and resuspended in mTeSR1 supplemented with Rock inhibitor (S1049, Selleck Chemicals) at 10uM final concentration. When the colonies that expressed mCherry reached the size of a nickel, they were marked and picked in Matrigel coated 24-well plates.

Endogenous OCT4 levels. Endogenous OCT4 levels in H9 wild-type cells and H9 OCT4-mCherry clone 8-2 were determined by antibody staining using a rabbit anti-OCT4 antibody (ab19857, Abcam). Immunostaining was performed using standard protocols. Briefly, cells were fixed for 15 min in 4% paraformaldehyde and permeabilized and blocked for 30 minutes in 5% goat serum with 0.3% Triton X-100 in TBS. Incubation with primary antibody was performed overnight and the incubation with the secondary antibody (Molecular Probes) was done at room temperature for 45 minutes. Nuclei were visualized using NucBlue Fixed Cell Stain ready Probes reagent (R37606, Molecular Probes).

Live-cell imaging analysis. Asynchronous H9 OCT4-mCherry cells were plated on 12-well glass bottom plates (Cellvis) in phenol-red free or clear DMEM/F-12 (Gibco) supplemented with mTeSR1 supplement (05850, STEMCELL Technologies) approximately 24 hours before being

bioRxiv preprint doi: https://doi.org/10.1101/137299; this version posted May 12, 2017. The copyright holder for this preprint (which was not certified by peer review) is the author/funder, who has granted bioRxiv a license to display the preprint in perpetuity. It is made available under aCC-BY 4.0 International license.

imaged. Cells were imaged using a Nikon Ti Eclipse microscope operated by NIS Elements software V4.30.02 with an Andor ZYLA 4.2 cMOS camera and a custom stage enclosure (Okolabs) to ensure constant temperature, humidity, and CO2 levels. Fresh media with or without BMP4 was added every 24 h. Images were flat-field corrected using NIS Elements.

Image analysis. A custom ImageJ plugin (available upon request) was used to perform automated segmentation and manually tracking of hESCs. Fluorescence intensity was quantified using an adapted threshold followed by watershed segmentation of the OCT4-mCherry channel. The program tracked the cell ID, parent ID, frame number, mean intensity and exported this information to MATLAB for analysis.

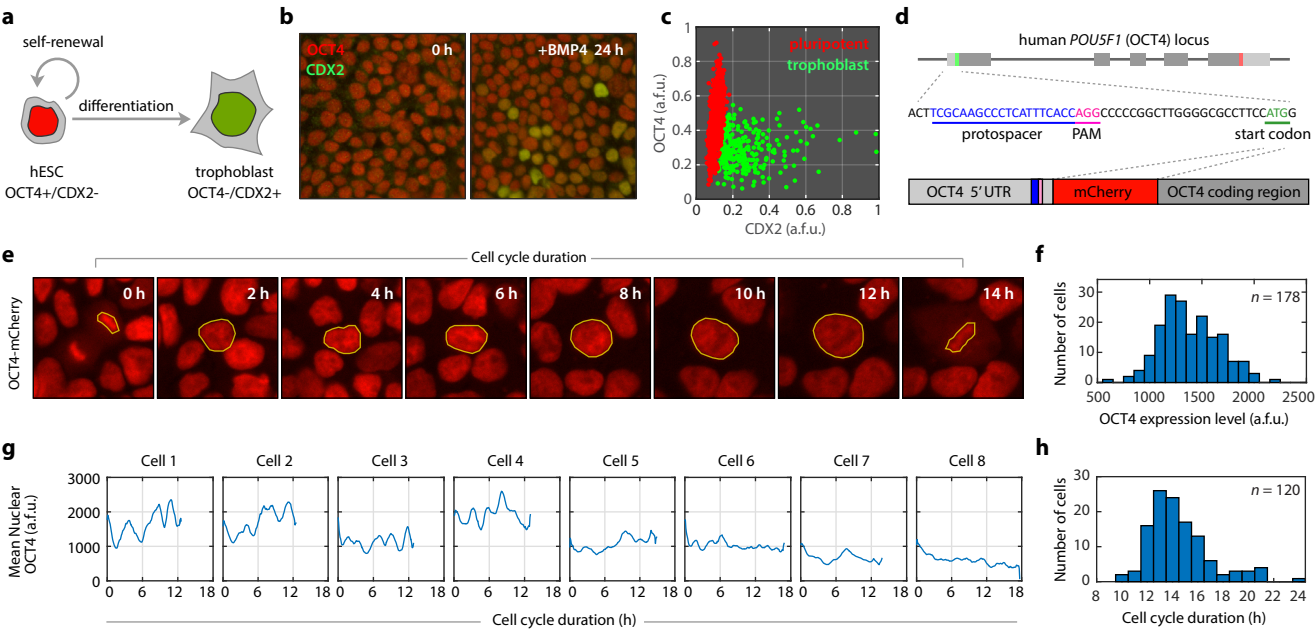

Figure 1 | Single-cell dynamics of OCT4 in human embryonic stem cells. a, Individual hESCs have the potential to generate another stem cell through self-renewal or to differentiate into a more lineage-specific cell type. The first fate decision during human development leads to separation of a pluripotent inner cell mass (OCT4+/CDX2-) and a population of differentiated trophoblast cells (OCT4-/CDX2+). **b**, Before differentiation, hESCs show uniform expression of OCT4. Treatment with BMP4 produces a mixture of OCT4+/CDX2- pluripotent hESCs and OCT4-/CDX2+ trophoblast cells. **c**, Quantification of OCT4 and CDX2 expression by immunofluorescence after 24 h of BMP4 treatment reveals two populations of hESCs. Cells were assigned to one of two distinct populations based on a 2-component mixed Gaussian distribution (Extended Data Fig. 6). **d**, A fluorescent mCherry coding sequence was introduced into endogenous OCT4 locus of H9 hESCs using CRISPR-mediated homologous recombination. **e**, Filmstrip of OCT4 dynamics in an undifferentiated hESC throughout its cell cycle duration. Yellow outlines indicate the region used to quantify mean nuclear fluorescence intensity. **f**, Distribution of OCT4 levels in individual hESCs. A single OCT4 level was quantified for each cell by averaging the mCherry intensity over the lifetime of the cell. **g**, Single-cell traces of OCT4 signaling. The length of each cell's trace indicates its cell cycle duration. **h**, Distribution of cell cycle durations for 120 hESCs.

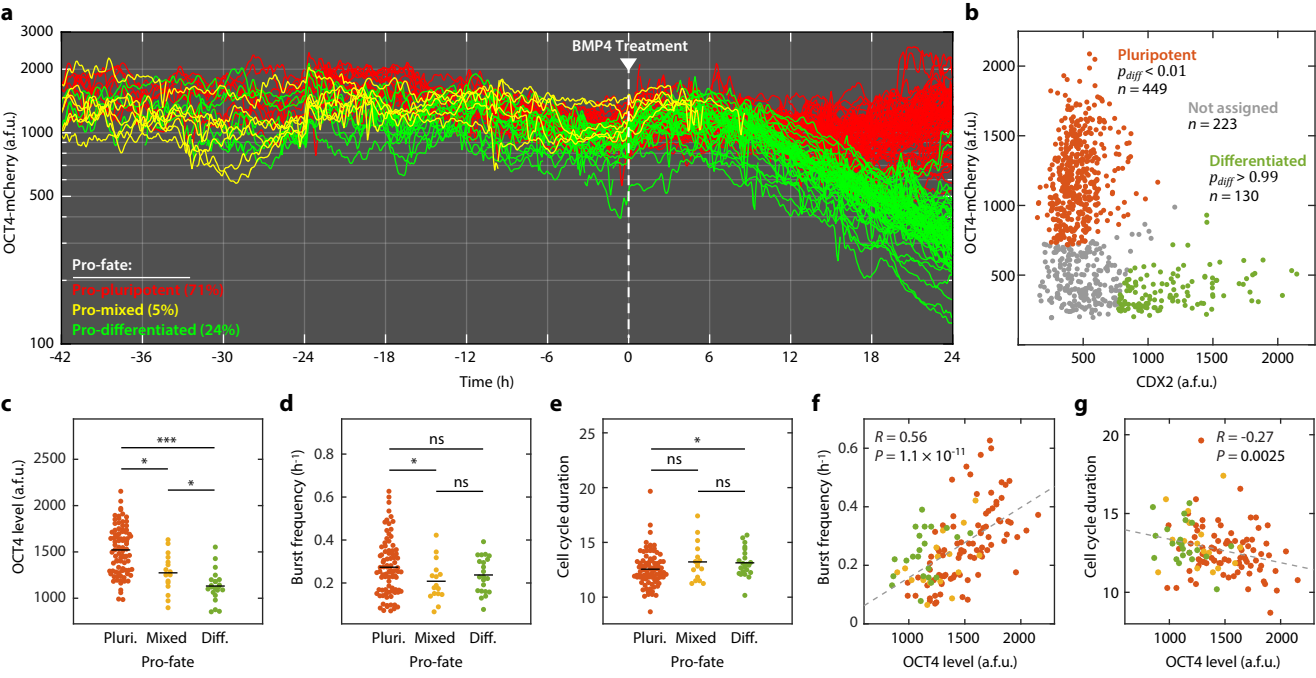

Figure 2 | Preexisting differences in OCT4 dynamics predict eventual fate decisions. a, Single-cell traces of hESCs before and after treatment with 100 ng/mL BMP4. Cells were imaged for 42 h prior to BMP4 treatment. Mean nuclear OCT4 levels were quantified every 5 minutes and individual cells were tracked from the cell division event that created the cell until its own division. **b,** 24 h after BMP4 treatment, cells were fixed, stained for expression of CDX2, and returned to the microscope for registration with the final time-lapse image. Mean nuclear OCT4-mCherry and CDX2 were quantified for each cell, and the resulting distribution was fit to a 2-component mixed Gaussian distribution representing pluripotent (OCT4+/CDX2-) and differentiated (OCT4-/CDX2+) cells (Extended Data Fig. 6). hESCs that could be assigned to either distribution with >99% confidence (red and green dots, $p_{diff} < 0.01$ or $p_{diff} > 0.99$) were considered for pro-fate analysis. Cells that did not reach this threshold (gray dots) were not used to determine pro-fate. Because cells in the final frame were assigned to only pluripotent or differentiated categories, pro-mixed cells (yellow traces in panel **a**) do not persist to the final frame. **c,** Distributions of OCT4 levels in pro-pluripotent, pro-mixed, and pro-differentiated cell populations. **d,** Distributions of OCT4 burst frequencies in pro-pluripotent, pro-mixed, and pro-differentiated cell populations. **e,** Distributions of cell cycle durations in pro-pluripotent, pro-mixed, and pro-differentiated cell populations. To gain an unbiased look at preexisting determinants of cell fate in panels **d**-**e**, only cells who completed their entire cell cycle duration before BMP4 addition (t = 0) were included in the analysis. **f,** Correlation between OCT4 level and burst frequency across the entire population of pro-fate cells. **g,** Correlation between OCT4 level and cell cycle duration across the entire population of pro-fate cells. * $P < 0.05$, ** $P < 0.005$, *** $P < 0.0005$; ns, not significant. *R*, Pearson correlation; *P*, *P*-value.

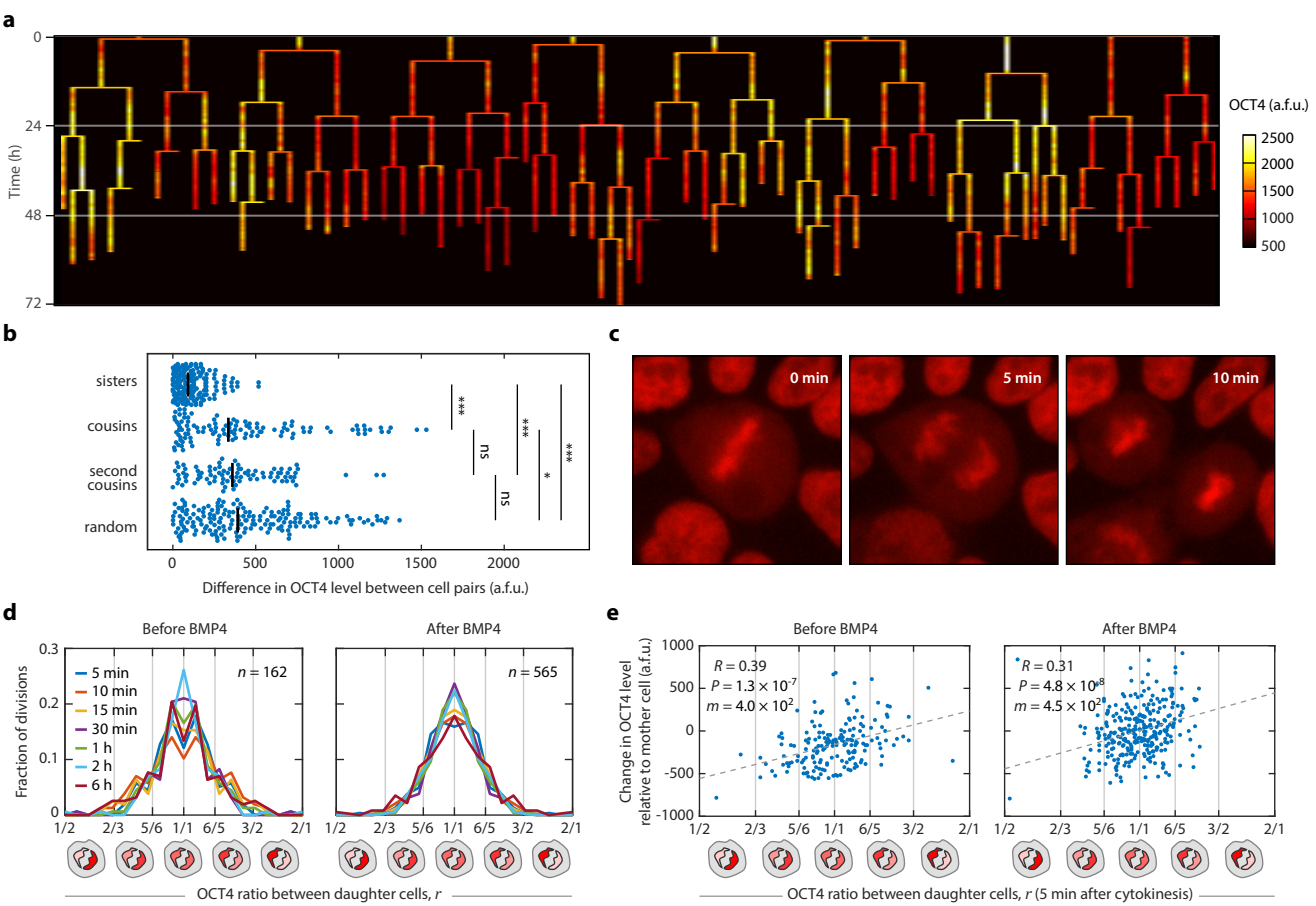

Figure 3 | Differences in OCT4 expression levels arise through asymmetric distribution of OCT4 to daughter cells. a, Lineage of OCT4 expression dynamics. Mean nuclear OCT4 levels were quantified in individual hESCs continuously for 72 h under undifferentiated conditions. Vertical bars represent individual cells. Thin horizontal bars denote cell division events. Color scale indicates low (*black*), intermediate (*red*), and high (*white*) OCT4 expression levels. **b,** Differences in OCT4 levels between sister cells, cousin cells, second cousin cells, and randomly paired cells. **c,** Filmstrip showing distribution of OCT4 to daughter cells during cell division. **d,** Distribution of OCT4 ratios between sister cells before and after BMP4 treatment. Ratios for both sister cells (r and $1/r$) are plotted to emphasize symmetry. Differently colored curves represent the distribution of ratios at different time points after division. For time points after 5 minutes, the ratio was determined by first calculating a mean OCT4 level for each sister cell among all previous time points and then calculating the resulting ratio between sisters. **e,** Correlation between OCT4 ratio established within 5 minutes of cell division and the final OCT4 level. To avoid trivial correlations, OCT4 measurements used to determine the ratio (x-axis) were excluded from the final OCT4 level calculation (y-axis). * $P < 0.05$, *** $P < 0.0005$, two-sample Kolmogorov-Smirnov test; ns, not significant. R, Pearson correlation; P, P-value; m, slope of best fit line.

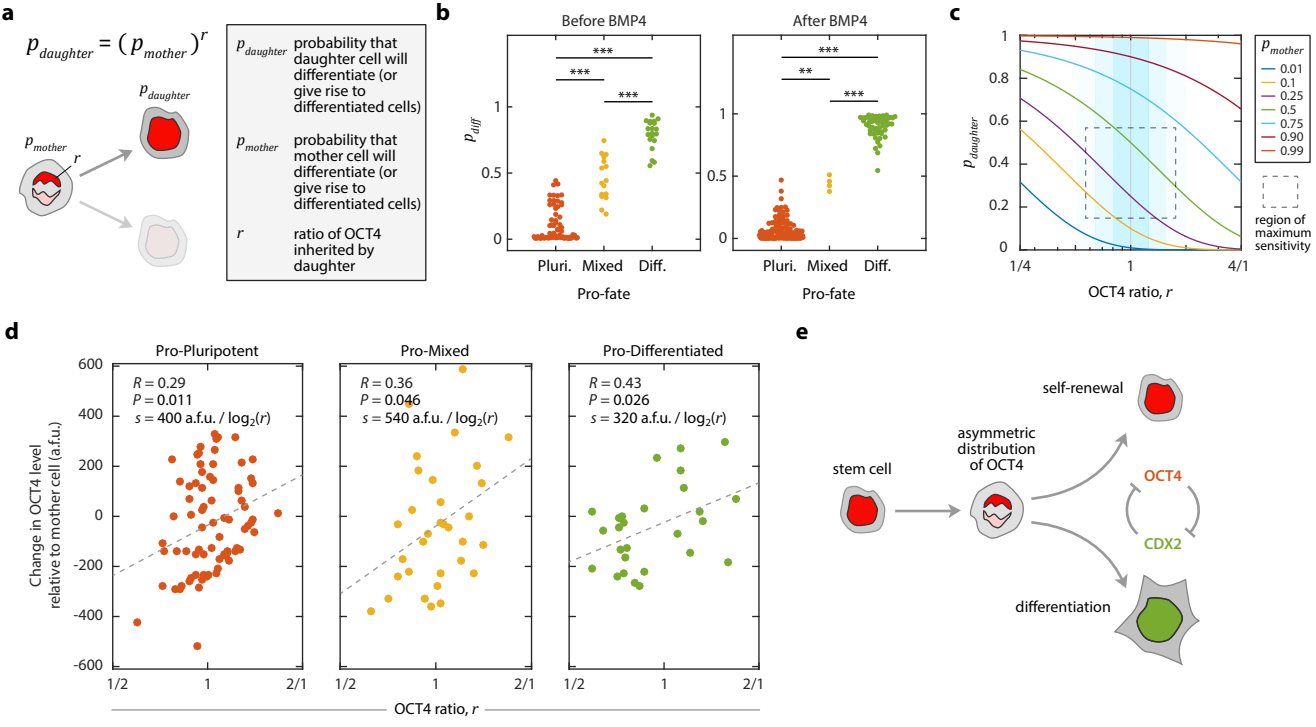

Figure 4 | Ratiometric distribution of OCT4 during cell division alters the balance between self-renewal and differentiation. a, Formula that describes how the differentiation probability of a daughter cell $p_{daughter}$ depends on the differentiation probability of the mother cell p_{mother} and the inherited ratio of OCT4, r. **b,** Equation 1 was used recursively to assign a differentiation probability to each cell based on the final measured differentiation probabilities p_{diff} (see Fig. 2b) and the inherited ratio of OCT4 for each cell. Cells are grouped according to their experimentally determined pro-fate. **c,** Theoretical predictions of Equation 1 for multiple values of maternal differentiation probability p_{mother}. The line is steepest at $p_{mother} = 1/e \approx 0.368$. **d,** Sensitivity of pro-fate groups to inherited OCT4 ratio. The change in final OCT4 levels is plotted against the ratio of OCT4 inherited in pro-pluripotent, pro-mixed, or pro-differentiated populations. **e,** Model for stem cell fate decisions altered by asymmetric distribution of OCT4 during cell division. ** $p < 0.005$, *** $p < 0.0005$. R, Pearson correlation; P, P-value; s, slope of best fit line representing sensitivity to r.

bioRxiv preprint doi: https://doi.org/10.1101/137299; this version posted May 12, 2017. The copyright holder for this preprint (which was not certified by peer review) is the author/funder, who has granted bioRxiv a license to display the preprint in perpetuity. It is made available under aCC-BY 4.0 International license.

Extended Data for:

Ratiometric distribution of OCT4 during stem cell division controls the balance between self-renewal and differentiation

Samuel C. Wolff[1]*, Raluca Dumitru[1]*, Cierra D. Dungee[1], Katarzyna M. Kedziora[1], Rachel A. Haggerty[2], JrGang Cheng[3], Adriana S. Beltran[1], and Jeremy E. Purvis[1,2,4,†]

[1]Department of Genetics
[2]Curriculum for Bioinformatics and Computational Biology
[3]UNC Neuroscience Center
[4]Lineberger Comprehensive Cancer Center

University of North Carolina, Chapel Hill
120 Mason Farm Road
Chapel Hill, NC 27599-7264

*These authors contributed equally

[†]Corresponding Author:
Jeremy Purvis
Genetic Medicine Building 5061, CB#7264
120 Mason Farm Road
Chapel Hill, NC 27599-7264
jeremy_purvis@med.unc.edu

bioRxiv preprint doi: https://doi.org/10.1101/137299; this version posted May 12, 2017. The copyright holder for this preprint (which was not certified by peer review) is the author/funder, who has granted bioRxiv a license to display the preprint in perpetuity. It is made available under aCC-BY 4.0 International license.

CONTENTS

Figure 1 | hESCs with high OCT4 expression after BMP4 treatment are competent to differentiate into multiple cell types. 3

Figure 2 | BMP4 induces a radially symmetric differentiation pattern 4

Experimental methods for constructing the H9 OCT4-mCherry cell line 5

Figure 3 | OCT4-mCherry shows accurate co-localization, degradation kinetics, and chromatin binding patterns compared to endogenous OCT4 protein 6

Figure 4. Cells bearing the OCT4-mCherry reporter are competent to differentiate into multiple cell types 8

Figure 5 | Proliferation of hESCs as a function of light exposure sampling rate and intensity 10

Figure 6 | Classification of cell fates using a 2-component Gaussian distribution 11

Figure 7 | Difference in OCT4 levels is strongly correlated with number of cell divisions separating two cells 12

Figure 8 | OCT4 ratios are not correlated with nuclear area or radial position within the colony 13

Figure 9 | The inherited ratio of OCT4 becomes more strongly correlated with final OCT4 level over time 14

Figure 10 | The ratio of OCT4 established immediately after cell division predicts the difference in final OCT4 expression between sister cell pairs.....15

bioRxiv preprint doi: https://doi.org/10.1101/137299; this version posted May 12, 2017. The copyright holder for this preprint (which was not certified by peer review) is the author/funder, who has granted bioRxiv a license to display the preprint in perpetuity. It is made available under aCC-BY 4.0 International license.

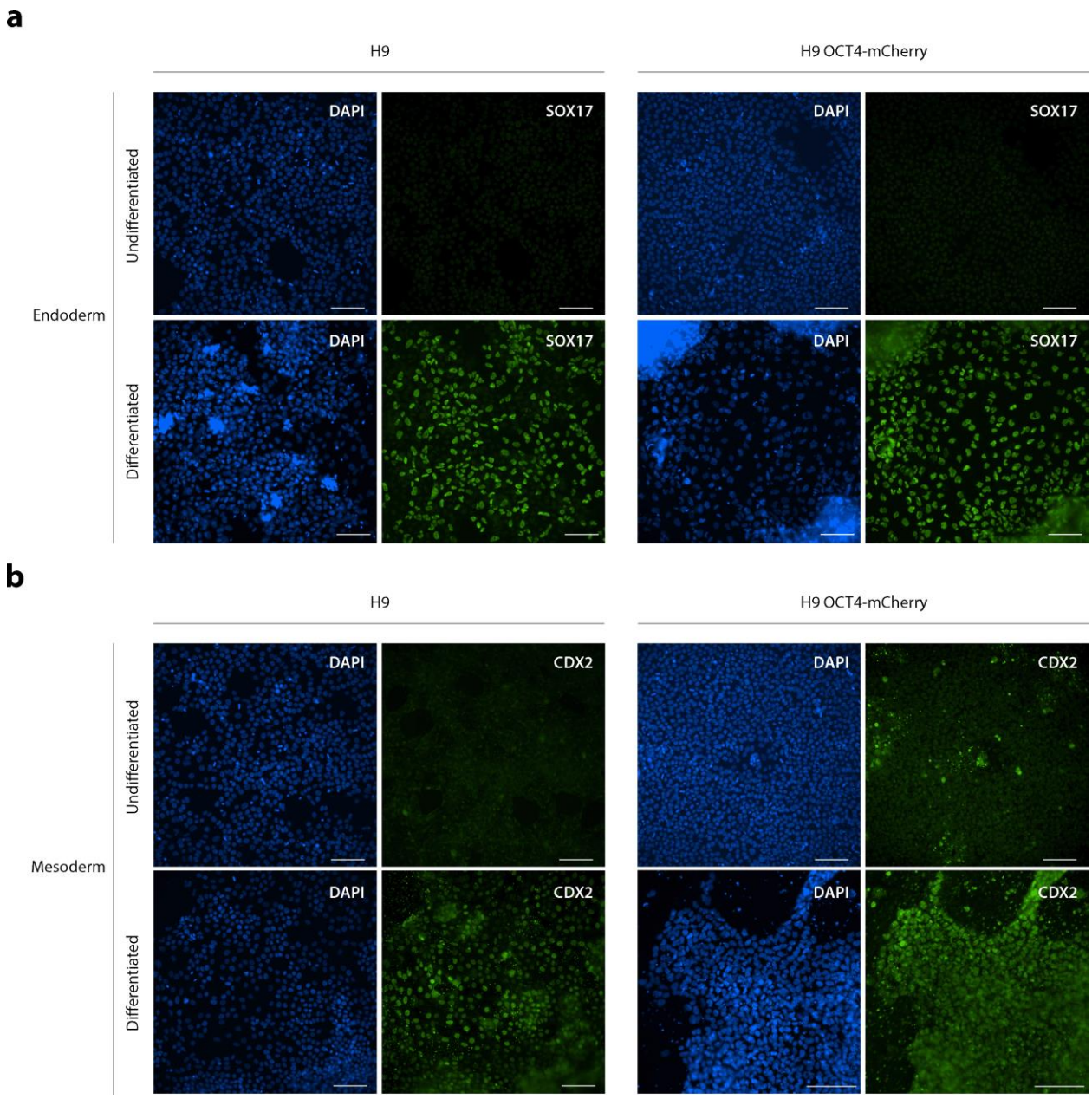

Figure 1 | hESCs with high OCT4 expression after BMP4 treatment are competent to differentiate into multiple cell types. H9 wild-type and H9 OCT4-mCherry cells were seeded at a density of 2×10^5 cells/cm^2. After 1 d, cells were treated with 100 ng/ml BMP4 (Peprotech). After 24 hours, the center "core" of each colony (see **Figure 2**) was manually removed and placed on Matrigel-coated 24-well glass bottom plates. Cells were allowed to adhere for 2 hours and then differentiated toward **a,** endoderm or **b,** mesoderm using the STEMdiff™ Trilineage Differentiation Kit (STEMCELL Technologies). Scale bar = 100 µm.

bioRxiv preprint doi: https://doi.org/10.1101/137299; this version posted May 12, 2017. The copyright holder for this preprint (which was not certified by peer review) is the author/funder, who has granted bioRxiv a license to display the preprint in perpetuity. It is made available under aCC-BY 4.0 International license.

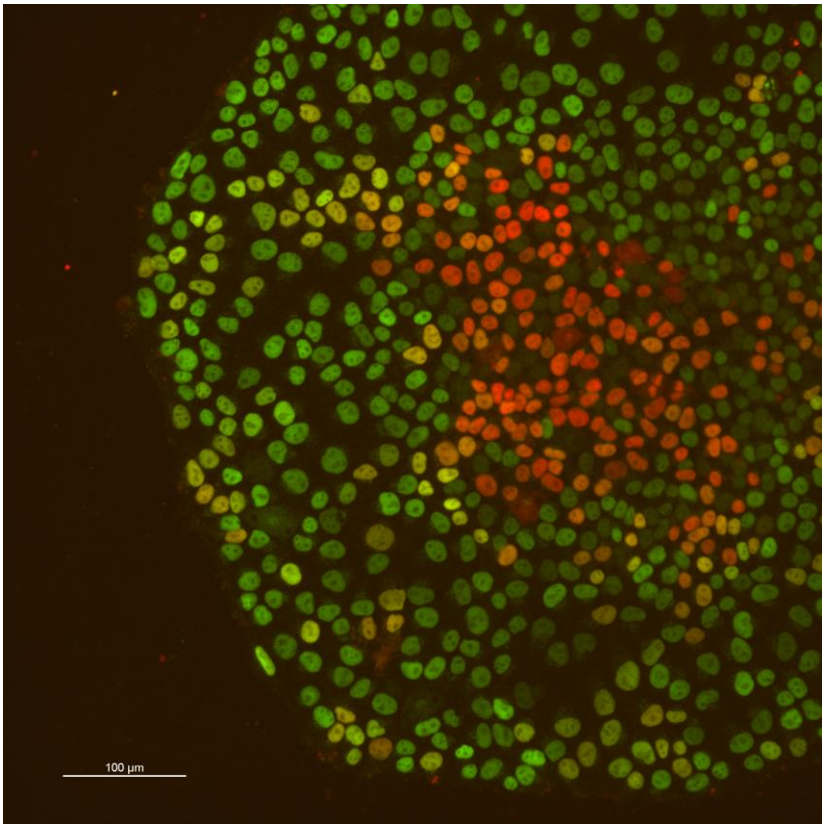

Figure 2 | BMP4 induces a radially symmetric differentiation pattern. H9 OCT4-mCherry cells were treated with 100 ng/mL BMP4 for 24 h. Merged image shows OCT4-mCherry expression (*red*) and antibody-labeled CDX2 expression (*green*).

bioRxiv preprint doi: https://doi.org/10.1101/137299; this version posted May 12, 2017. The copyright holder for this preprint (which was not certified by peer review) is the author/funder, who has granted bioRxiv a license to display the preprint in perpetuity. It is made available under aCC-BY 4.0 International license.

Experimental methods for constructing the H9 OCT4-mCherry cell line

Guide RNA and CRISPR/Cas9 cutting vector. The gRNA sequence GTGAAATGAGGGCTTGCGA, targeting the start codon of human *POU5F1* (OCT4), was cloned into pX330 (AddGene) using the standard cloning protocol described Ran et al[1]. The cutting efficiency of the Cas9/OCT4-gRNA was validated with Guide-it Mutation Detection Kit (Takara Bio).

Donor cassette construction. The 5' homology arm of OCT4 was amplified out of H9 genomic DNA with the following primers (Fwd: 5'-AAGGTTGGGAAACTGAGGCC-3', Rev: 5'-GGGAAGGAAGGCGCCCCAAG-3) yielding a 1114 bp homology arm that was then cloned into the pGEMTEZ plasmid (Promega) followed by the coding sequence for the mCherry fluorescent protein (minus its stop codon) followed by a short linker sequence (TCC GGA TCC) and the start ATG codon for OCT4. The OCT4 gene constituted the 3' homology arm and was amplified out of H9 genomic DNA with the following primers (Fwd: 5'- ATGGCGGGACACCTGGCTTC-3', Rev: 5- AGCTTTCTACAAGGGGTGCC-3') yielding a 1082 bp homology arm.

Introduction of exogenous DNA into H9 cells. H9 cells were cultured on 10 cm dishes and, when 80% confluent, were dissociated using 0.5mM EDTA. 10×10^6 cells were resuspended in 800 µL ice-cold PBS containing 25 µg of the OCT4-mCherry donor vector and 25 µg of the guideRNA/Cas9 vector. Cells were electroporated in 100 µL tips (Neon, ThermoFisher Scientific) using program 19 of the optimization protocol (1050V, 30ms, 2 pulses) and resuspended in mTeSR1 (STEMCELL Technologies) supplemented with Rock inhibitor (S1049, Selleck Chemicals) at a final concentration of 10 µM. When colonies that expressed mCherry reached the size of a nickel, they were marked and picked into Matrigel coated 24-well plates.

bioRxiv preprint doi: https://doi.org/10.1101/137299; this version posted May 12, 2017. The copyright holder for this preprint (which was not certified by peer review) is the author/funder, who has granted bioRxiv a license to display the preprint in perpetuity. It is made available under aCC-BY 4.0 International license.

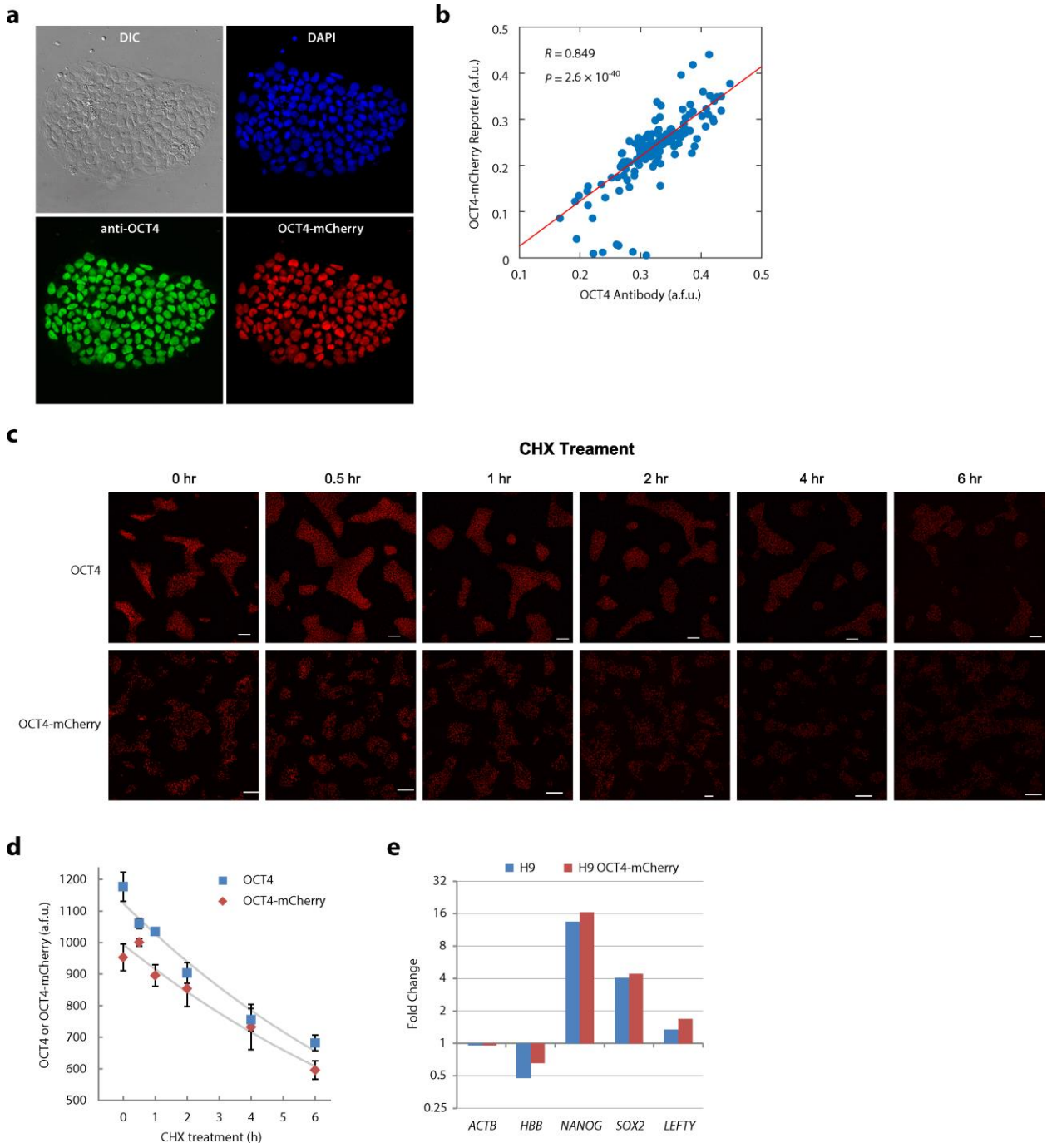

Figure 3 | OCT4-mCherry shows accurate co-localization, degradation kinetics, and chromatin binding patterns compared to endogenous OCT4 protein.

a, Colony of clonal hESCs expressing OCT4-mCherry. **b,** Correlation between OCT4-mCherry reporter and endogenous OCT4 in single cells. Cells from Panel A were segmented and mean fluorescence intensity was quantified using CellProfiler[2]. **c,** H9 or H9-OCT4-mCherry cells were seeded at a density of 3.75×10^4 cell/cm^2 in 12-well plates using mTeRS1 medium

bioRxiv preprint doi: https://doi.org/10.1101/137299; this version posted May 12, 2017. The copyright holder for this preprint (which was not certified by peer review) is the author/funder, who has granted bioRxiv a license to display the preprint in perpetuity. It is made available under aCC-BY 4.0 International license.

supplemented with 5 μM Y-27632 dihydrochloride ROCK inhibitor (STEMCELL Technologies). After 1 d, cells were treated with 50 μg/mL cyclohexamide for the indicated times and either imaged immediately (H9-OCT4-mCherry) or prepared for immunofluorescence imaging (H9). **d,** Mean fluorescence intensity was quantified for individual cells using Nikon Elements analysis software, and a mean-population intensity was calculated for each field of view by averaging the mean nuclear intensities over all cells in the field. Each data point is the average mean-population intensity of 3 fields of view, each containing approximately 1500 cells. Background-subtracted values were fit to an exponential function to yield half-life estimates of 8.65 ± 2.23 h for endogenous OCT4 and 7.34 ± 1.10 h for OCT4-mCherry. **e,** Enrichment of gene promoter regions for H9 hESCs and H9 OCT4-mCherry cell lines. Chromatin immunoprecipitation for OCT4 was performed as described by Jung et al[3]. Primers for promoter regions were *ACTB*: ACTCGAGAGAG and CTACTACTCTAC; *HBB*: ACTCGAGAGAG and CTACTACTCTAC; *NANOG*: ACTCGAGAGAG and CTACTACTCTAC; *SOX2*: ACTCGAGAGAG and CTACTACTCTAC; and *LEFTY*: *ACTB*: ACTCGAGAGAG and CTACTACTCTAC.

bioRxiv preprint doi: https://doi.org/10.1101/137299; this version posted May 12, 2017. The copyright holder for this preprint (which was not certified by peer review) is the author/funder, who has granted bioRxiv a license to display the preprint in perpetuity. It is made available under aCC-BY 4.0 International license.

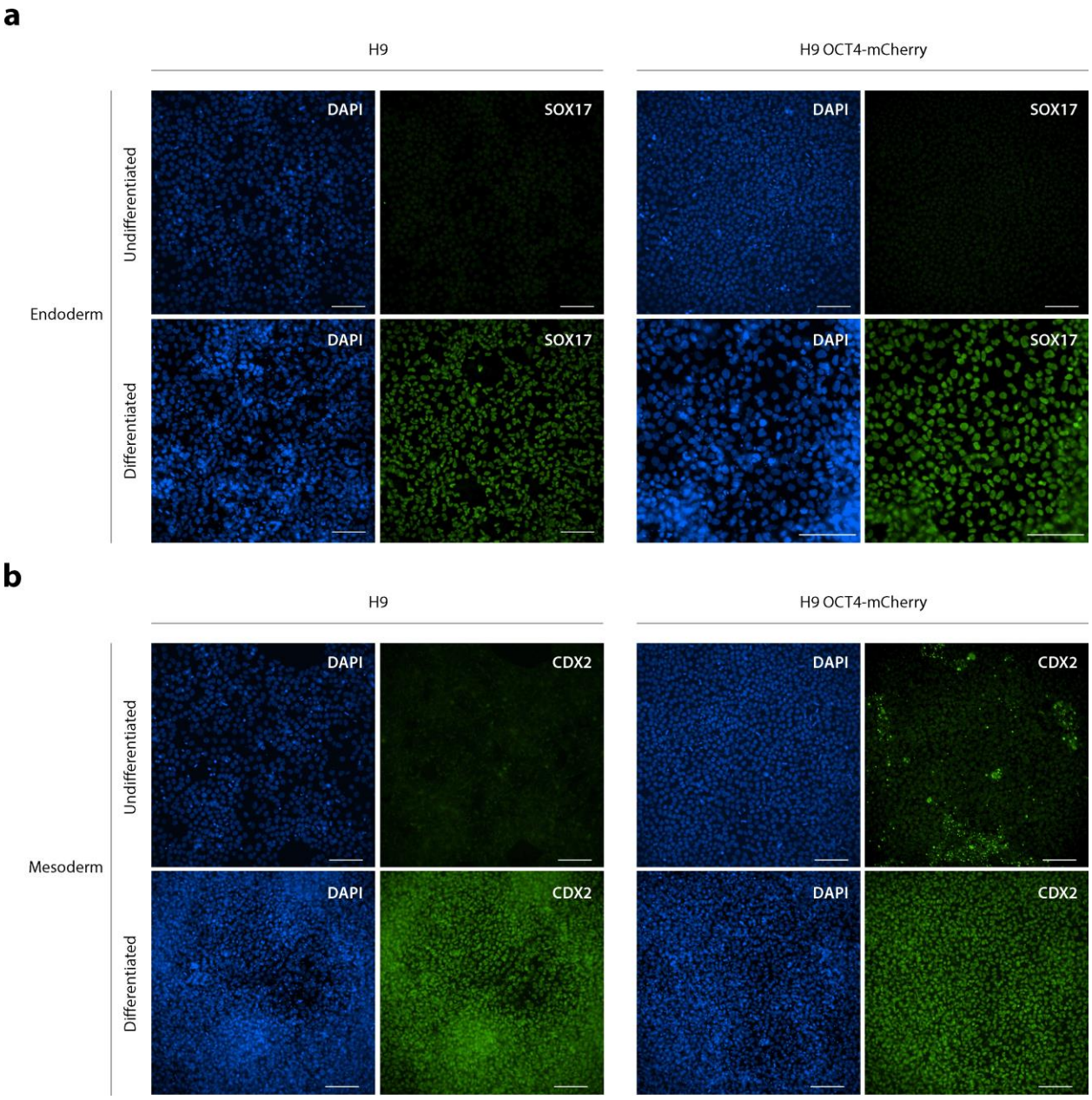

Figure 4 | Cells bearing the OCT4-mCherry reporter are competent to differentiate into multiple cell types. H9 wild-type and H9 OCT4-mCherry clone 8-2 cells were seeded at the density of 2×10^5 cell/cm^2 for endoderm and 5×10^4 cell/cm^2 for mesoderm lineage differentiation on 24-well glass bottom plates using mTeRS1 medium supplemented with 5 µM Y27632 (STEMCELL Technologies). After 24 hours, cells were differentiated into **a,** endoderm or **b,** mesoderm using the STEMdiff™ Trilineage Differentiation kit (STEMCELL Technologies). Medium was replaced every day for 5 days, then cells were fixed 15 min with 4% paraformaldehyde, permeabilized for 15 min with 0.3% Triton X-100 and blocked 1 hour with 5% BSA at room temperature. Then, cells differentiated to endoderm were incubated with SOX17

bioRxiv preprint doi: https://doi.org/10.1101/137299; this version posted May 12, 2017. The copyright holder for this preprint (which was not certified by peer review) is the author/funder, who has granted bioRxiv a license to display the preprint in perpetuity. It is made available under aCC-BY 4.0 International license.

(Abcam), and cells differentiated to mesoderm were incubated with CDX2 (Abcam), overnight. Cells were incubated with secondary antibody for 1 hour at room temperature. Nuclei were visualized with NucBlue Fixed Cell Stain ready Probes reagent (Molecular Probes). Scale bar = 100 μm.

bioRxiv preprint doi: https://doi.org/10.1101/137299; this version posted May 12, 2017. The copyright holder for this preprint (which was not certified by peer review) is the author/funder, who has granted bioRxiv a license to display the preprint in perpetuity. It is made available under aCC-BY 4.0 International license.

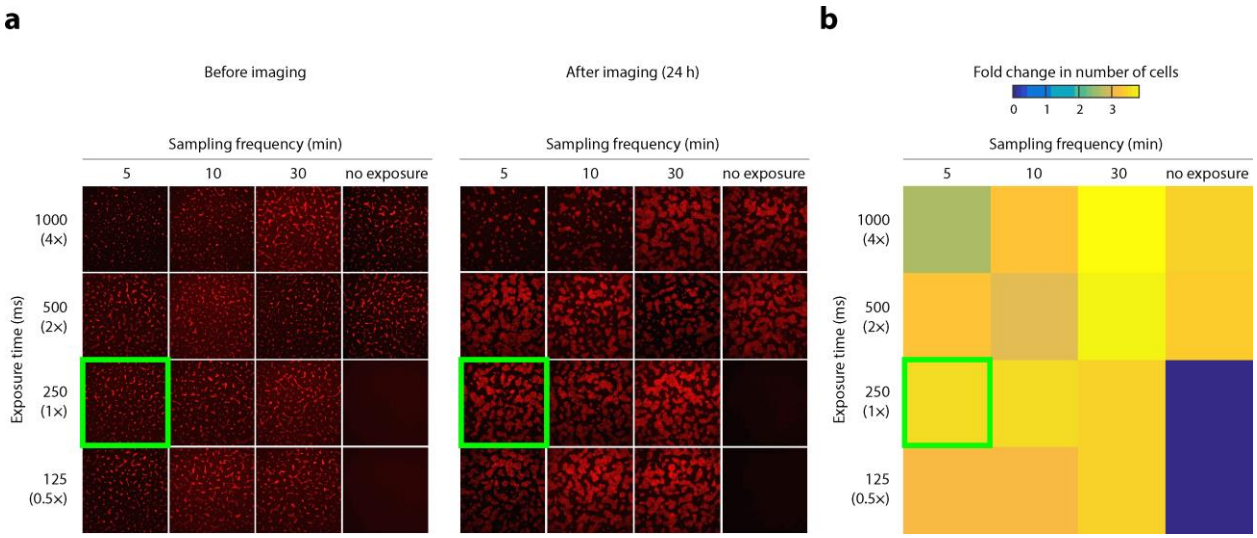

Figure 5 | Proliferation of hESCs as a function of light exposure sampling rate and intensity. a, H9 OCT4-mCherry cells were seeded onto glass bottom dishes and subjected to time-lapse fluorescence imaging for 24 h at the indicated exposure durations and sampling frequencies. For each condition, a single image was captured by the camera both before and after light exposure to determine the extent of cell proliferation. Nikon Elements spot detection algorithm was used to count nuclei before and after imaging for each condition. In the fourth column, cells were not exposed to any light other than during the first and last image captured for quantification of cell proliferation. The green box indicates the exposure setting used in this study. **b,** Heat map showing the fold change in the number of nuclei quantified for each condition.

bioRxiv preprint doi: https://doi.org/10.1101/137299; this version posted May 12, 2017. The copyright holder for this preprint (which was not certified by peer review) is the author/funder, who has granted bioRxiv a license to display the preprint in perpetuity. It is made available under aCC-BY 4.0 International license.

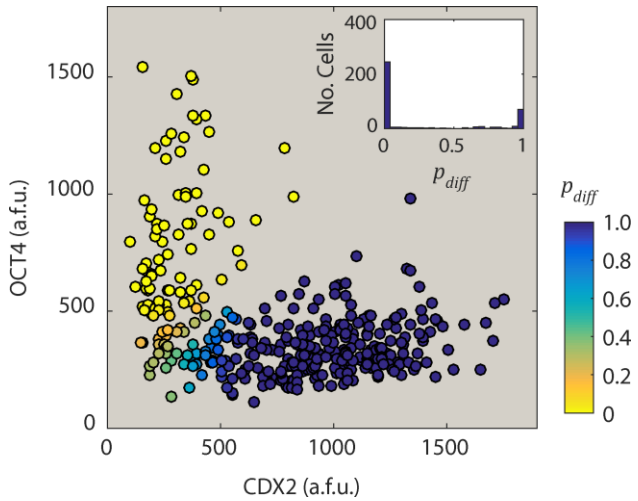

Figure 6 | Classification of cell fates using a 2-component Gaussian distribution. Mean nuclear intensity values for OCT4 and CDX2 were used to separate the population of cells into two groups using a mixed Gaussian model. *Inset*, distribution of posterior probabilities (p_{diff}) for all cells. Only cells that could be confidently labeled as pluripotent (p_{diff}<0.01) or differentiated (p_{diff}> 0.99) were considered for pro-fate analysis. Similar class assignments were made by employing *k*-means clustering with *k* = 2.

bioRxiv preprint doi: https://doi.org/10.1101/137299; this version posted May 12, 2017. The copyright holder for this preprint (which was not certified by peer review) is the author/funder, who has granted bioRxiv a license to display the preprint in perpetuity. It is made available under aCC-BY 4.0 International license.

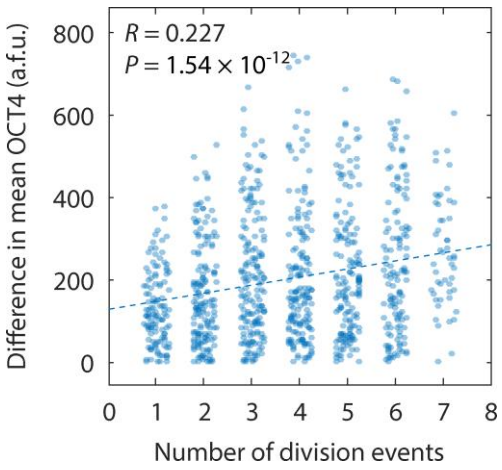

Figure 7 | Difference in OCT4 levels is strongly correlated with number of cell divisions separating two cells. All pairs of cells in Figure 3a from the main text were compared for difference in OCT4 level (*y-axis*) and number of cell division events separating those cells (*x-axis*). For example, mother and daughter cell pairs are separated by 1 cell division event, whereas cousin cells are separated by 3 division events. As the number of division events increases, the difference in OCT4 levels off because each division event is equally likely to increase or decrease the difference in OCT4 levels between two given cells.

bioRxiv preprint doi: https://doi.org/10.1101/137299; this version posted May 12, 2017. The copyright holder for this preprint (which was not certified by peer review) is the author/funder, who has granted bioRxiv a license to display the preprint in perpetuity. It is made available under aCC-BY 4.0 International license.

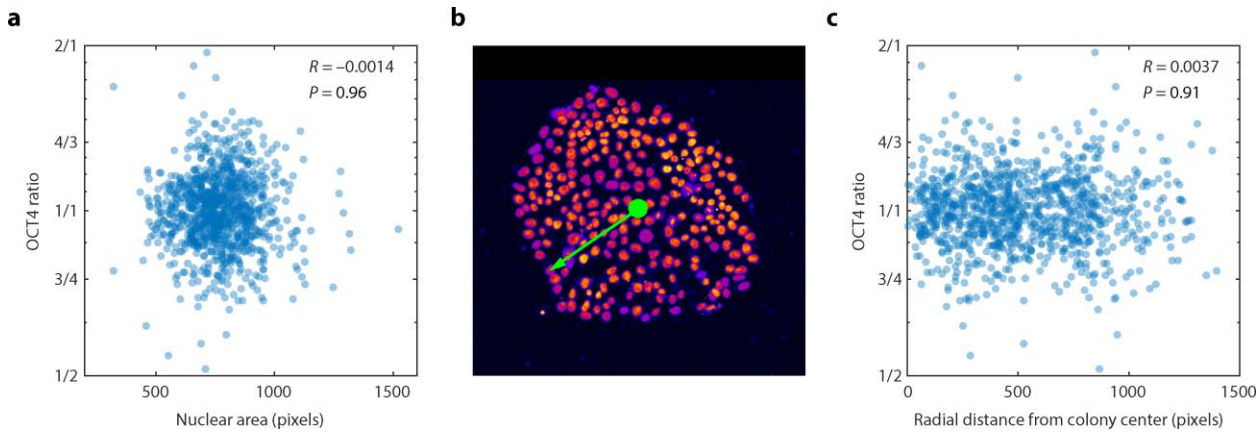

Figure 8 | OCT4 ratios are not correlated with nuclear area or radial position within the colony. a, Scatter plot of OCT4 ratio as a function of nuclear area for sister cells. To avoid noise due to segmentation errors, nuclear area was calculated 25 min after cell division, when OCT4 became diffuse throughout the nucleus. **b,** The colony center was defined as a center of mass of all OCT4-expressing cells. The radial position of individual cells was defined as a distance (in pixels) between the center of a cell and the center of the colony. **c,** Scatter plot of OCT4 ratio as a function of radial distance from the center of the colony.

bioRxiv preprint doi: https://doi.org/10.1101/137299; this version posted May 12, 2017. The copyright holder for this preprint (which was not certified by peer review) is the author/funder, who has granted bioRxiv a license to display the preprint in perpetuity. It is made available under aCC-BY 4.0 International license.

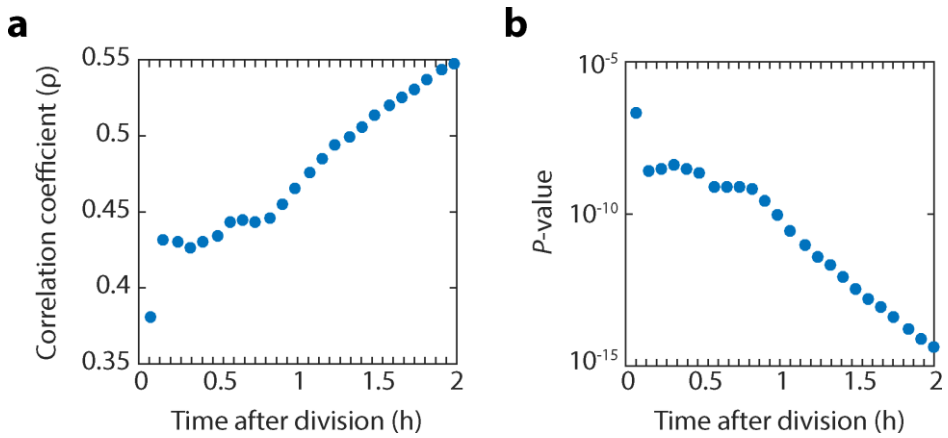

Figure 9 | The inherited ratio of OCT4 becomes more strongly correlated with final OCT4 level over time. a, Correlation of OCT4 ratio between sister cells and differences in final OCT4 levels. At each time point, the ratio of OCT4 between sister cell pairs was calculated as the ratio of the cumulative sum of mean OCT4 intensity values at all preceding time points. This ratio was used to predict the final OCT4 level for each cell, calculated as the cumulative sum of mean intensities for the remaining time points. **b,** Corresponding *P*-values for correlation in panel **a**.

bioRxiv preprint doi: https://doi.org/10.1101/137299; this version posted May 12, 2017. The copyright holder for this preprint (which was not certified by peer review) is the author/funder, who has granted bioRxiv a license to display the preprint in perpetuity. It is made available under aCC-BY 4.0 International license.

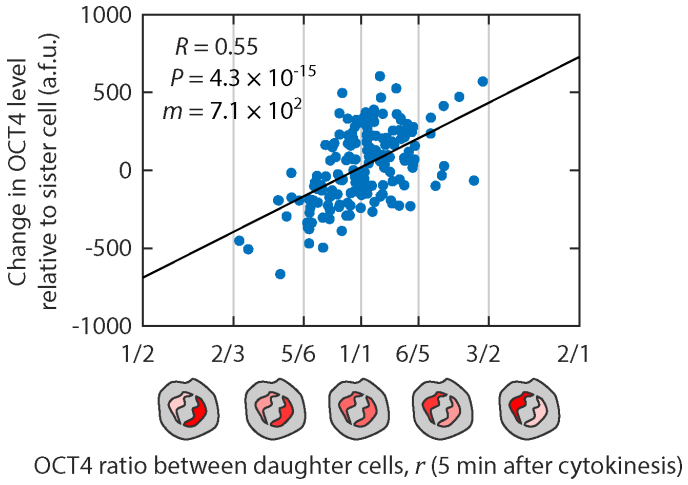

Figure 10 | The ratio of OCT4 established immediately after cell division predicts the difference in final OCT4 expression between sister cell pairs. OCT4 ratios between sister cell pairs were calculated within 5 minutes of the beginning of anaphase. Differences in mean OCT4 levels between sister-cell pairs were calculated as described in **Fig. 1** of the main text.

bioRxiv preprint doi: https://doi.org/10.1101/137299; this version posted May 12, 2017. The copyright holder for this preprint (which was not certified by peer review) is the author/funder, who has granted bioRxiv a license to display the preprint in perpetuity. It is made available under aCC-BY 4.0 International license.

REFERENCES

1 Ran, F. A. *et al.* Genome engineering using the CRISPR-Cas9 system. *Nature protocols* **8**, 2281-2308, doi:10.1038/nprot.2013.143 (2013).

2 Carpenter, A. E. *et al.* CellProfiler: image analysis software for identifying and quantifying cell phenotypes. *Genome Biol* **7**, R100, doi:10.1186/gb-2006-7-10-r100 (2006).

3 Jung, M. *et al.* A data integration approach to mapping OCT4 gene regulatory networks operative in embryonic stem cells and embryonal carcinoma cells. *PLoS One* **5**, e10709, doi:10.1371/journal.pone.0010709 (2010).